JOURNAL OF SOLID STATE CHEMISTRY 105, 271–278 (1993)

Phase Transition and V^{4+}–V^{4+} Pairing in VO_2(B)

YOSHIO OKA,* TAKESHI YAO,† AND NAOICHI YAMAMOTO

Department of Chemistry, College of Liberal Arts and Sciences, and †Department of Industrial Chemistry, Faculty of Engineering, Kyoto University, Kyoto 606, Japan

AND YUTAKA UEDA AND AKIHIKO HAYASHI

Institute for Solid State Physics, University of Tokyo, Tokyo 106, Japan

Received August 3, 1992; in revised form November 5, 1992; accepted November 11, 1992

The study of low-temperature X-ray diffraction and magnetic properties of VO_2(B) has revealed a structural phase transition and formation of V^{4+} ion pairs. The phase transition occurs over a temperature range from 300 to 180 K; however, a complete structural change is not attained. The low-temperature phase has the same monoclinic symmetry as the high-temperature phase. The X-ray Rietveld refinements revealed a significant decrease in the V(2)–V(2) distance from 0.2867 to 0.2670 nm, indicating V^{4+}–V^{4+} pairing for half of the V sites in the low-temperature phase. The pairing has been confirmed by the observation of a spin-singlet state in the ^{51}V NMR measurements and corresponds to the decrease in magnetic susceptibility. The behavior of phase transition and pairing in VO_2(B) are analogous to those in V_6O_{13}, which has a related structure.

Introduction

Pairing of V^{4+} ions develops in vanadium oxides such as rutile-type VO_2, V_6O_{13}, and V_4O_7, where crystallographic distortions and/or drastic changes in electrical conductivity are somtimes involved. Rutile-type VO_2 exhibits a first-order metal–insulator (M–I) transition at 340 K (*1*). On the transition the regular rutile structure of the high-temperature phase is distorted into a monoclinic one due to the formation of V^{4+}–V^{4+} pairs along the *c*-axis of the rutile lattice (*2*). V_6O_{13} undergoes an M–I transition at 150 K accompanied by a slight lattice distortion from $C2/m$ to Cm (*3*). A ^{51}V NMR study (*4*) has proved the occurrence of V^{4+}–V^{4+} pairing in half of the V^{4+} sites, although a low-temperature single-crystal X-ray study (*3*) failed to assign the ion-pairing sites. V_4O_7 is a member of the Magnéli phases and exhibits an M–I transition at 250 K (*5*). The triclinic lattice is maintained through the transition and the V^{4+}–V^{4+} pairing proceeds continuously with decreasing temperature.

V^{4+}–V^{4+} pairing seems likely to occur in other crystallographic phases of VO_2, namely VO_2(A) and VO_2(B), which are metastable with respect to the equilibrium phase of rutile-type VO_2. In practice VO_2(A) exhibits a phase transition at 435 K and some experimental results suggest the possibility of ion pairing in the low-temperature phase (*6, 7*). VO_2(B) adopts a monoclinic structure $C2/m$ with $a = 1.203$, $b = 0.3693$, $c = 0.642$ nm, and $\beta = 106.6°$ (*8*). Since its structure is related to that of V_6O_{13} (*8, 9*), the pairing must be favorable in VO_2(B); however, no work has been done on this subject. The present study is focused on the formation of V^{4+}–V^{4+} pairs in VO_2(B). Low-temperature X-ray diffraction, magnetic susceptibility, and ^{51}V NMR

* Present address: Department of Natural Environment Sciences, Faculty of Integrated Human Studies, Kyoto University, Kyoto 606, Japan.

0022-4596/93 $5.00

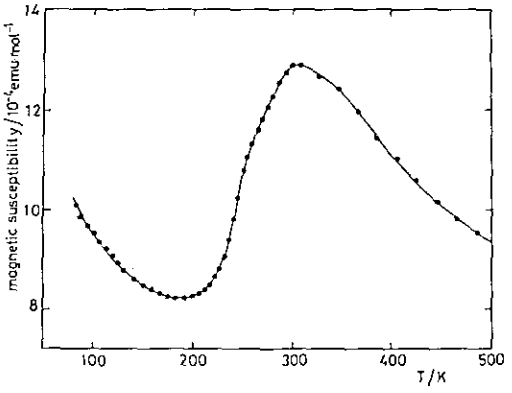

FIG. 1. Magnetic susceptibility vs temperature for $VO_2(B)$.

measurements were performed and structural analyses were made using the X-ray Rietveld method. As a result, a phase transition takes place and half of the V^{4+} ions form pairs in the low-temperature phase, analogously to the case of V_6O_{13}.

Experimental

$VO_2(B)$ samples in powder form were prepared hydrothermally using $VO(OH)_2$ as a starting material. The details of the sample preparation were described elsewhere (*10*). The sample powders were ground to diminish preferred orientation, which yielded a small amount of the $VO_2(A)$ phase due to a mechanochemical phase transition (*10*). X-ray diffraction (XRD) patterns were taken with monochromatized Cu$K\alpha$ radiation by using a Mac Science MXP[18] system. The low-temperature X-ray measurements were performed at several temperatures ranging from 50 to 300 K using a closed-cycle helium refrigerator. The sample powders were mixed with Apiezon grease and pasted onto a stainless sample holder. The XRD measurements at 50 and 300 K were made by a step-scanning method in a 2θ range from 12° to 115° and with a step width of 0.02° and a step time of 10 sec. For measurements at other temperatures a 2θ range from 12° to

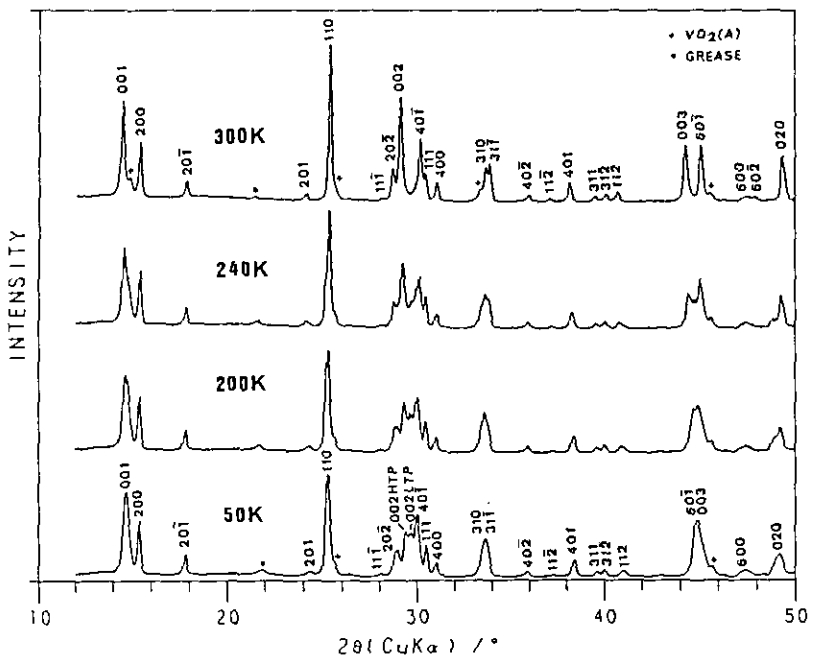

FIG. 2. X-ray diffraction patterns for $VO_2(B)$ at 300, 240, 200, and 50 K. The peaks at 300 K and 50 K are indexed for the HTP and the LTP, respectively.

57° and a step time of 2 sec were employed. The procedure of the X-ray Rietveld analysis was basically the same as that employed in the previous studies (*7*, *11*) but was modified for solving multiphasic systems. Magnetic susceptibility measurements were carried out using a torsion magnetic balance from 77 to 700 K. ^{51}V NMR measurements were carried out at room temperature and 77 K by using a standard phase-coherent pulsed type spectrometer at a fixed frequency of 16.2400 MHz.

Results

Figure 1 shows the temperature dependence of magnetic susceptibility χ for VO_2(B). The profile of the χ–T curve, unlike that of ordinary paramagnets, has a peak around 300 K and a minimum around 180 K. The gradual decrease of χ below 300 K may be due to some structural transition. Figure 2 shows changes in XRD patterns with temperature below 300 K. The pattern at 300 K is the same as that reported (*8*) except for the presence of small peaks of VO_2(A) phase. The gradual changes in the patterns below 300 K are indicative of a transition to a new phase. The phase at 300 K and the new phase below 300 K are designated as the high-temperature phase (HTP) and the low-temperature phase (LTP), respectively. As demonstrated by the pattern at 50 K of Fig. 2, the peaks of the LTP can be indexed in the same monoclinic system as that of the HTP. Close examination of the changes in XRD patterns reveals the presence of the residual HTP down to 50 K as exemplified in Fig. 2 by the 002 HTP peak at 50 K. Figure 3 shows temperature variations of the unit cell constants: a contraction of the *c*-axis, expansions of the *a*- and *b*-axis, and an increase in the monoclinic angle β occur on the transition from the HTP to the LTP.

The Rietveld analysis has been performed on the multiphasic systems consisting of HTP and VO_2(A) at 300 K, and of LTP, HTP, and VO_2(A) at 50 K. Based on the crystal structure determined by Théobald

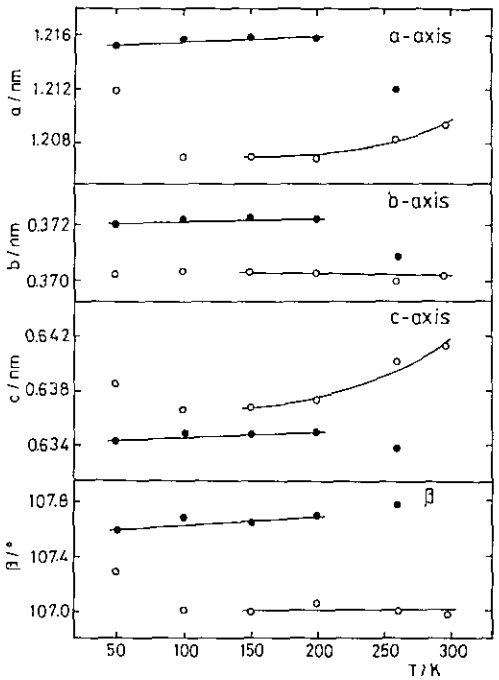

FIG. 3. Unit cell parameters vs temperature for VO_2(B). Open and closed circles represent the HTP and the LTP, respectively.

et al. (*8*), the structure of the HTP was refined using the XRD data at 300 K, leading to the *R* factors $R_{wp} = 0.106$ and $R_p = 0.118$. Assuming that the LTP is isostructural with the HTP, the structure of the LTP was refined using the XRD data at 50 K, leading to $R_{wp} = 0.113$ and $R_p = 0.118$, where the atomic parameters of the HTP were fixed to the values obtained at 300 K. As for the minor VO_2(A) phase, the unit cell parameters were refined using the literature values (*7*) for the atomic parameters. The results of the Rietveld refinement plots are illustrated in Fig. 4. The crystallographic data and the atomic parameters for the HTP at 300 K and the LTP at 50 K are listed in Tables I and II, respectively. Table III compares the V–V distances through shared VO_6 octahedral edges. It should be noted that the shortest $V(2)^{i}$–$V(2)^{ii}$ distance (0.2867 nm) in the HTP further shortens to 0.2670 nm in the LTP while other V–V dis-

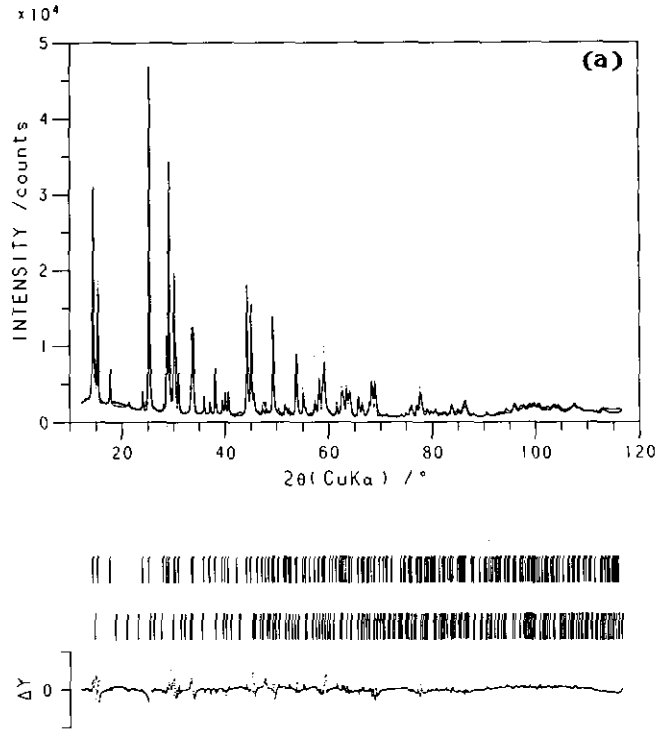

FIG. 4. Rietveld refinement plots for VO_2(B): (a) 300 K and (b) 50 K. The calculated and observed patterns are shown by solid lines and dots, respectively. The vertical marks denote positions of Bragg reflections: (a) the HTP (top) and VO_2(A) (bottom); (b) the LTP (top), the HTP (middle), and VO_2(A) (bottom). The traces in the bottoms are plots of the difference: observed minus calculated.

tances are almost unchanged. This is indicative of V^{4+} ion pairing in V(2) sites. Figure 5 visualizes the structural difference between the HTP and the LTP, where slight changes in the frameworks of VO_6 octahedra as well as the displacements of V sites are seen. Figure 6 shows a temperature dependence of the relative amount of the LTP which is saturated below 150 K at about 70%. Pairing of V^{4+} ions results in a singlet-spin state which is detectable by the ^{51}V NMR measurements. As shown in Fig. 7, a signal with a positive Knight shift of +0.20% was clearly observed at 77 K, while no signal was observed at room temperature. According to the extensive NMR studies on vanadium oxides (*12–15*), unpaired V^{4+} ions with $3d^1$ moments exhibit negative Knight shifts due to the negative core-polarization fields and fast relaxation rates, while paired V^{4+} ions in singlet spin states exhibit positive Knight shifts and slow relaxation rates. The positive Knight shift observed in the LTP of VO_2(B) therefore indicates the presence of singlet spin V^{4+} pairs which are assigned to V(2)–V(2) sites.

TABLE 1

CRYSTALLOGRAPHIC DATA FOR HTP OF VO_2(B)

	HTP	LTP
T/K	300	50
Space group	$C2/m$	$C2/m$
a/nm	1.2093(1)	1.2152(2)
b/nm	0.37021(2)	0.37199(5)
c/nm	0.64330(5)	0.6347(1)
β/°	106.97(1)	107.58(3)
V/nm^3	0.27455(6)	0.2735(2)

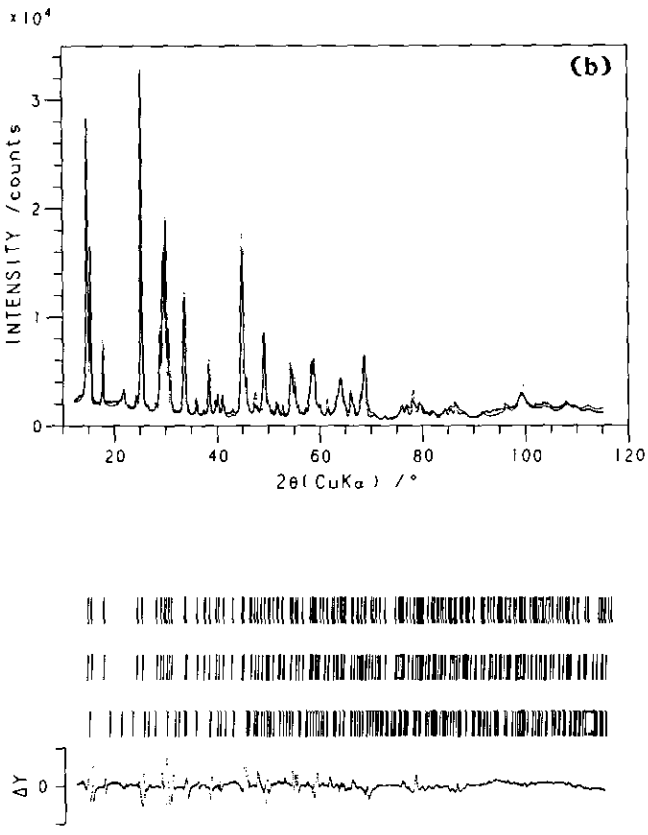

FIG. 4—*Continued*

Discussion

Phase transitions and V^{4+}–V^{4+} pairing in VO_2(B) have been revealed experimentally. V^{4+} ion pairs are formed in V(2) sites in the *ac*-plane and thus half of the V atoms in the LTP form pairs. The transition from the HTP to the LTP starts at about 300 K and proceeds gradually toward 180 K, accompanied by slight changes in unit cell con-

TABLE II

ATOMIC PARAMETERS IN HTP AND LTP OF VO_2(B)

		HTP		LTP	
Atom	Position	*x*	*z*	*x*	*z*
V(1)	4*i*	0.3010(2)	0.7214(4)	0.2964(3)	0.7249(7)
V(2)	4*i*	0.3995(2)	0.3145(4)	0.4040(4)	0.3281(6)
O(1)	4*i*	0.3601(6)	1.0006(13)	0.3512(11)	0.9944(24)
O(2)	4*i*	0.2338(6)	0.3436(11)	0.2328(12)	0.3502(19)
O(3)	4*i*	0.4432(7)	0.6496(12)	0.4401(12)	0.6545(21)
O(4)	4*i*	0.1212(5)	0.6928(10)	0.1046(11)	0.6792(18)

TABLE III

V–V DISTANCES (nm) IN HTP AND LTP OF VO_2(B)

	HTP	LTP
$V(1)^{i}$–$V(1)^{iv}$	0.3319(4)	0.3307(6)
$V(1)^{i}$–$V(2)^{ii}$	0.3177(4)	0.3169(6)
$V(1)^{i}$–$V(2)^{iv}$	0.3005(4)	0.3002(6)
$V(2)^{i}$–$V(2)^{ii}$	0.2867(4)	0.2670(7)

Note. Symmetry codes: i x, 0, z; ii $1 - x$, 0, $1 - z$; iii $\frac{1}{2} + x$, $\frac{1}{2}$, z; iv $\frac{1}{2} - x$, $\frac{1}{2}$, $1 - z$.

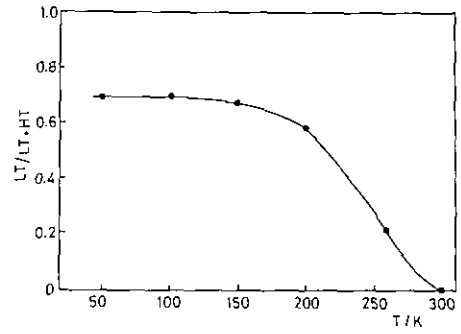

FIG. 6. Temperature dependence of the volume fraction of the LTP.

stants and no lattice distortion. Finally, about 30% of the HTP survive below 150 K. The behavior of the transition is thus somewhat different from that in rutile-type VO_2 and V_6O_{13}, which exhibit a sharp and complete transition together with a lattice distortion. The anomalous temperature dependence of χ in Fig. 1 is now accounted for as follows. The increase with temperature from 500 to 300 K is due to the paramagnetic V atoms of the HTP and the effective moment is estimated to be 2.0 μ_B. The decrease with temperature from 300 to 180 K is attributed to the formation of nonmagnetic V–V pairs and the increase below 180 K to the paramagnetic V atoms in both the LTP and the residual HTP.

The V–V distances in VO_2(B) are comparable to those in the rutile-type VO_2 (*16*). The shortest V–V distance in the HTP of VO_2(B) is 0.2867 nm for V(2)–V(2) which is close to the distance of 0.287 nm in the rutile-type VO_2 where 3*d* electrons are itinerant. It is noted that both V–V distances are less than the Goodenough critical separation R_c of 0.294 nm for localized vs itinerant 3*d* electrons in oxides for V^{4+} ions (*16*). This indicates that the V(2)–V(2) interaction in VO_2(B), in analogy with the rutile-type VO_2, becomes a covalent bond with decreasing temperature resulting in V^{4+}–V^{4+} pairing. In practice the V(2)–V(2) distance shortens to 0.2670 nm in the LTP, which is again close to the shorter V–V distance

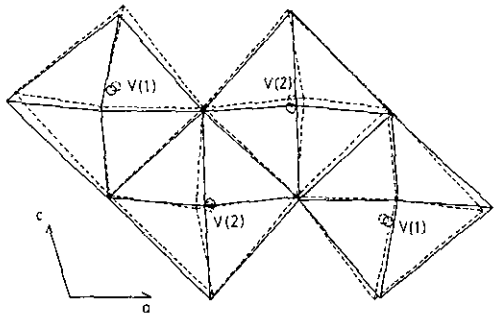

FIG. 5. VO_6 octahedral frameworks in the *ac*-plane for VO_2(B). The frameworks for the LTP and the HTP are drawn by solid and broken lines, respectively. V sites of the LTP are represented by solid open circles and those of the HTP by broken circles.

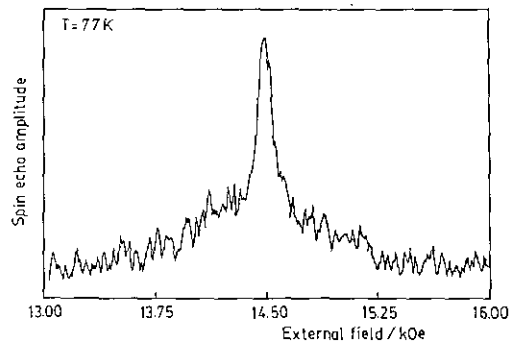

FIG. 7. ^{51}V NMR spectrum for VO_2(B) operated at 16.2400 MHz and taken at 77 K.

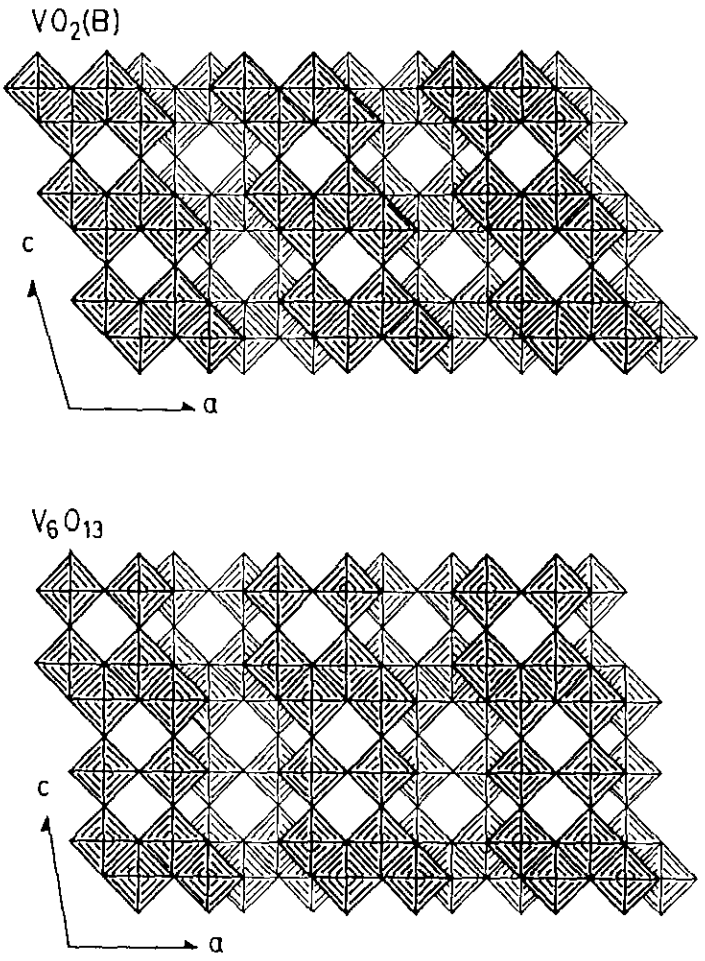

FIG. 8. Diagrammatic illustrations of the structures of VO_2(B) (top) and V_6O_{13} (bottom).

of 0.265 nm in rutile-type VO_2, where V–V pairs are formed.

It is worthwhile to describe the analogy between VO_2(B) and V_6O_{13} with regard to the V^{4+}–V^{4+} pairing. As shown in Fig. 8, both oxides bear a strong structural similarity, with the same space group $C2/m$. The structure of V_6O_{13} consists of two types of VO_6 octahedral arrays running along the a-axis: single VO_6 array and edge-shared double VO_6 array (*9*). By removal of the single VO_6 arrays the structure of V_6O_{13} is converted into that of VO_2(B). The crystallographic and NMR studies (*3, 4*) on V_6O_{13} showed that V atoms in the double VO_6 arrays become V^{4+}-like and those in the single VO_6 arrays become V^{5+}-like in the LTP and half of the V^{4+}-like atoms undergo singlet-spin pairing. This ionic arrangement in the double VO_6 arrays of the LTP V_6O_{13} corresponds exactly to that of VO_2(B). The variations in the unit cell parameters of the phase transition for both oxides are also similar; that is, expansions of the a- and b-axes, a contraction of the c-axis, and an increase of the monoclinic angle (Ref. (*3*) and Fig. 2). Therefore, the mechanism of pairing in VO_2(B) must be similar to that in V_6O_{13}. The present study has located the V sites forming pairs as depicted in Fig. 5; presumably this result may be applicable to V_6O_{13}, in which the pairing sites have not been specified.

Acknowledgments

We are grateful to Professors N. Soga, K. Kosuge, and F. Takei for valuable discussions and continuous encouragement, to Professor H. Yasuoka for NMR measurements, and to Professor T. Ohtani for magnetic susceptibility measurements. Thanks are also due to the Computer Center, Institute for Molecular Science, Okazaki National Research Institutes for the use of the HITAC M-680H and S-820/80.

References

1. F. J. Morin, *Phys. Rev. Lett.* **3,** 34 (1959).
2. J. B. Goodenough, *Phys. Rev.* **117,** 1442 (1960).
3. P. D. Dernier, *Mater. Res. Bull.* **9,** 955 (1974).
4. M. Itoh, H. Yasuoka, Y. Ueda, and K. Kosuge, *J. Phys. Soc. Jpn.* **53,** 1847 (1984).
5. J. L. Hodeau and M. Marezio, *J. Solid State Chem.* **23,** 253 (1978).
6. Y. Oka, T. Ohtani, N. Yamamoto, and T. Takada, *Seramikkusu Ronbunshi* **97,** 1134 (1989).
7. Y. Oka, T. Yao, and N. Yamamoto, *J. Solid State Chem.* **86,** 116 (1990).
8. F. Théobald, R. Cabala, and J. Bernard, *J. Solid State Chem.* **17,** 431 (1976).
9. K. A. Wilhelmi, K. Waltersson, and L. Kihlborg, *Acta Chem. Scand.* **25,** 2675 (1971).
10. Y. Oka, T. Yao, and N. Yamamoto, *J. Mater. Chem.* **1,** 815 (1991).
11. Y. Oka, T. Yao, and N. Yamamoto, *J. Solid State Chem.* **89,** 372 (1990).
12. A. C. Gossard, J. P. Remeika, T. M. Rice, H. Yasuoka, K. Kosuge, and S. Kachi, *Phys. Rev. B* **9,** 1230 (1974).
13. A. C. Gossard, F. J. DiSalvo, L. C. Erich, J. P. Remeika, H. Yasuoka, K. Kosuge, and S. Kachi, *Phys. Rev. B* **10,** 4178 (1974).
14. K. Takanashi, H. Yasuoka, Y. Ueda, and K. Kosuge, *J. Phys. Soc. Jpn.* **52,** 3953 (1983).
15. S. Kachi, Y. Ueda, K. Kosuge, Y. Kitaoka, and H. Yasuoka, "Ferrites: Proceeding of the International Conference," pp. 131–134 (1980).
16. J. B. Goodenough, *J. Solid State Chem.* **3,** 490 (1971).